Transport studies in three-terminal microwave graphs with orthogonal, unitary, and symplectic symmetry

A. M. Martínez-Argüello,[1] A. Rehemanjiang,[2] M. Martínez-Mares,[3] J. A. Méndez-Bermúdez,[1] H.-J. Stöckmann,[2] and U. Kuhl[4]

[1]*Instituto de Física, Benemérita Universidad Autónoma de Puebla, Apartado Postal J-48, 72570 Puebla, Pue., Mexico*

[2]*Fachbereich Physik der Philipps-Universität Marburg, D-35032 Marburg, Germany*

[3]*Departamento de Física, Universidad Autónoma Metropolitana-Iztapalapa, Apartado Postal 55-534, 09340 Ciudad de México, Mexico*

[4]*Université de Nice-Sophia Antipolis, Laboratoire de la Physique de la Matière Condensée, CNRS, Parc Valrose, 06108 Nice, France*

(Received 19 February 2018; revised manuscript received 8 August 2018; published 24 August 2018)

The Landauer-Büttiker formalism establishes an equivalence between the electrical conduction through a device, e.g., a quantum dot, and the transmission. Guided by this analogy we perform transmission measurements through three-port microwave graphs with orthogonal, unitary, and symplectic symmetry, thus mimicking three-terminal voltage drop devices. One of the ports is placed as input and a second one as output, while a third port is used as a probe. Analytical predictions show good agreement with the measurements in the presence of orthogonal and unitary symmetries, provided that the absorption and the influence of the coupling port are taken into account. The symplectic symmetry is realized in specifically designed graphs mimicking spin-1/2 systems. Again a good agreement between experiment and theory is found. For the symplectic case the results are marginally sensitive to absorption and coupling strength of the port, in contrast to the orthogonal and unitary case.

DOI: 10.1103/PhysRevB.98.075311

Wave transport and wave scattering phenomena have been of great interest in the last decades, both from experimental and theoretical points of view (see for instance Ref. [1]). Apart from the intrinsic importance in the complex scattering in a particular medium, the interest also comes from the equivalence between physical systems belonging to completely different areas, in which the dimensions of the systems may differ by several orders of magnitude [2]. One of these equivalences occurs in mesoscopic quantum systems, where the electrical conduction reduces to a scattering problem through the Landauer-Büttiker formalism [3–5]. Following this line, classical analogies of quantum systems have been used as auxiliary tools to understand the properties of the conductance of electronic devices in two-terminal configurations [6–10]. A plethora of chaotic scattering experiments in the presence of time reversal invariance (TRI) and no spin-1/2 have been performed [7,8,10–16], while very few experimental studies regarding absence of TRI are reported [7,8,17,18]. Furthermore, due to its intrinsic complexity, there are no scattering experiments up to now for systems with TRI and spin-1/2, where the signatures of the symplectic ensemble are expected, though there is one study of the spectral statistics in Au nanoparticles obeying this symmetry [19]. Moreover, very recently the appearance of a microwave experiment showing the signatures of the symplectic symmetry [20,21] for eigenvalue statistics has opened the possibility to study transport in the presence of this symmetry.

Multiterminal devices are good candidates to provide experimental realizations for the three symmetry classes: orthogonal, unitary, and symplectic. Alternatively to the most used two-terminal configuration, three-terminal systems provide information of nonlocal effects of transport observables. In the present paper we make theoretical predictions for coherent transport in a three-terminal quantum device. In the spirit of the mentioned classical analogy, we propose experimental realizations with microwave graphs, which represent experiments of transport in three-terminal systems for the three mentioned symmetry classes.

The electrical current I_i on the terminal i of an electronic device, as given by Büttiker's formula, can be written as [22]

$$I_i = \sum_j G_{ij}(V_i - V_j), \quad \text{with} \quad G_{ij} = \frac{e^2}{h} T_{ij}, \tag{1}$$

where V_i is the voltage at terminal i, and G_{ij} and T_{ij} are the conductance and transmission coefficient, respectively, from terminal j to terminal i. In a three-terminal configuration, one of the ports, let us say terminal 3, can be used as a probe by tuning its voltage to zero current. This voltage V_3 is a weighted average of the voltages in the other terminals, the weight being determined by the conductance coefficients from the other terminals to the probe [22]. It can be written as [4]

$$V_3 = \tfrac{1}{2}(V_1 + V_2) + \tfrac{1}{2}(V_1 - V_2)\, f, \tag{2}$$

where

$$f = \frac{T_{31} - T_{32}}{T_{31} + T_{32}}, \tag{3}$$

see Fig. 1. This equation shows that V_3 varies around the average of the voltages producing the bias V_1 and V_2. Hence, the quantity f takes values in the interval $[-1,\ 1]$ and contains all the information about the system. For instance, a three-terminal setting was considered in Refs. [23,24] to study the voltage drop along a disordered quantum wire.

Here we perform measurements of the quantity f through microwave graphs connected to three single channel ports: an input port, an output port, and a probe port. We focus here on the particular situation where the probe port is on one side

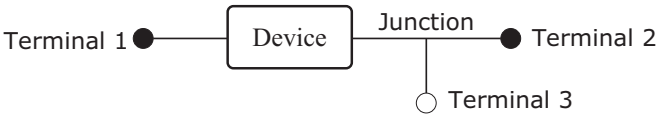

FIG. 1. Sketch of a three-terminal setting that allows the measurement of the voltage along a device. The device carries a current while the vertical wire measures the voltage drop. Thin lines represent perfect conductors connected to sources of voltages V_1, V_2, and V_3.

of the microwave graph, see Fig. 1. We study graphs with chaotic dynamics characterized by the orthogonal, unitary, and symplectic symmetries; labeled by $\beta = 1$, 2, and 4 in Dyson's scheme [25], respectively. The $\beta = 4$ case is realized in a network with specific properties that mimics a spin-1/2 system [20,21]. The fluctuations of f that arise when the frequency is varied are analyzed by means of random matrix theory (RMT) calculations. Analytical expressions for the distribution of f that describe the experiments for the three symmetry classes are verified by the measurements.

The experimental setup for $\beta = 2$ (with a small modification also for $\beta = 1$) is shown in Fig. 2. A chaotic microwave graph is formed by coaxial semirigid cables (Huber & Suhner EZ-141) with SMA connectors, coupled by T junctions at the nodes. An additional T junction at the exit port forms the three-terminal setting. For $\beta = 1$ all bonds were connected by T junctions, for $\beta = 2$ one of the T junctions was replaced by a circulator to break TRI. In both cases the found spectral level spacing distributions were in perfect agreement with the Wigner distributions for the Gaussian orthogonal ensemble (GOE) $\beta = 1$, and the Gaussian unitary ensemble (GUE) $\beta = 2$, respectively, see, e.g., Chap. 4.4 of Ref. [26]. The measurements were restricted to the operating range of the circulators (Aerotek I70-1FFF) from 6 to 12 GHz. To realize graphs showing the signatures of the Gaussian symplectic ensemble (GSE) $\beta = 4$, two copies of the graph shown in Fig. 2 are needed, where the implemented circulators lead to

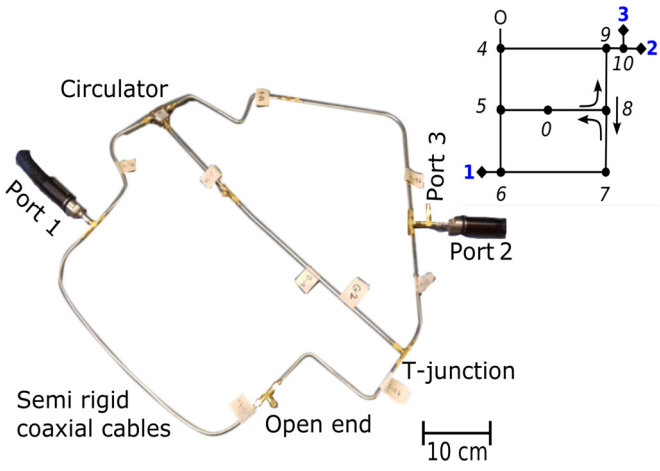

FIG. 2. Photograph of a three-port microwave graph with broken time reversal symmetry (GUE). The circulator in the graph adds directionality, breaking TRI, and yields to a GUE spectra. By replacing the circulator by an ordinary T junction, a graph with GOE spectra is obtained.

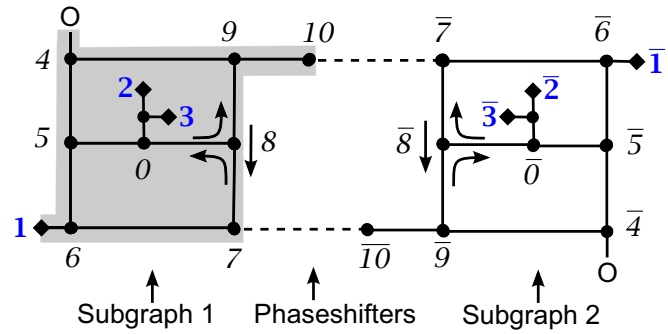

FIG. 3. Sketch of the three-terminal microwave GSE graph composed of two GUE subgraphs. The circulators in the graphs add directionality in the system, breaking TRI and yielding GUE spectra in each subgraph. Transmissions from ports 1 to 3, 1 to $\bar{3}$, $\bar{1}$ to 3, and from $\bar{1}$ to $\bar{3}$ are measured to obtain T_{31}. In a similar way, T_{32} is obtained.

an opposite sense of rotation. They are coupled by two bonds in an inversion symmetric geometry, with a phase shift of π in one of the bonds but not the other one, see Fig. 3. The whole graph obeys an antiunitary symmetry T, squaring to -1, thus mimicking a spin-1/2, see Ref. [20]. Transmission measurements were performed with an Agilent 8720ES vector network analyzer (VNA).

With respect to the quantity f, its fluctuations can be described by the scattering approach of RMT. Appealing to an ergodic hypothesis, fluctuations on the frequency are replaced by fluctuations on an ensemble of chaotic graphs, represented by an ensemble of scattering matrices. In the two-channel situation, the scattering matrix of the graph has the structure

$$S_g = \begin{pmatrix} r_g & t'_g \\ t_g & r'_g \end{pmatrix}, \tag{4}$$

where r_g (r'_g) and t_g (t'_g) are the reflection and transmission amplitudes, for incidence from the left (right). Depending on the symmetry class, S_g belongs to one of the circular ensembles: orthogonal (COE) for $\beta = 1$, unitary (CUE) for $\beta = 2$, and symplectic (CSE) for $\beta = 4$. The S_g matrix can be written in the polar representation as [27]

$$S_g = \begin{bmatrix} -\sqrt{1-\tau}\, e^{2i\phi'} & a^{-1}\sqrt{\tau}\, e^{i(\phi+\phi')} \\ a\sqrt{\tau}\, e^{i(\phi+\phi')} & \sqrt{1-\tau}\, e^{2i\phi} \end{bmatrix}, \tag{5}$$

where $0 \leqslant \tau \leqslant 1$, $0 \leqslant \phi$, $\phi' \leqslant \pi$, and a is a real, complex, or real quaternion number of modulus 1 for $\beta = 1$, 2, or 4, respectively. The probability density distribution of S_g is given by [27]

$$dP_\beta(S_g) = \frac{\beta}{2}\, \tau^{-1+\beta/2}\, d\tau \frac{d\phi}{\pi} \frac{d\phi'}{\pi} da. \tag{6}$$

The scattering matrix associated to the three-terminal setup of Fig. 1, where the probe is at the right of the graph, is given by [28]

$$S = S_{PP} + S_{PQ} S_0 \frac{1}{\mathbb{1}_3 - S_{QQ} S_0} S_{QP}, \tag{7}$$

where S_0 is the scattering matrix for the junction (see Fig. 1), $\mathbb{1}_3$ stands for the unit matrix of dimension 3, and

$$S_{\rm PP} = \begin{pmatrix} r_{\rm g} & 0 & 0 \\ 0 & 0 & 0 \\ 0 & 0 & 0 \end{pmatrix}, \quad S_{\rm PQ} = \begin{pmatrix} t'_{\rm g} & 0 & 0 \\ 0 & 1 & 0 \\ 0 & 0 & 1 \end{pmatrix}, \tag{8}$$

$$S_{\rm QP} = \begin{pmatrix} t_{\rm g} & 0 & 0 \\ 0 & 1 & 0 \\ 0 & 0 & 1 \end{pmatrix}, \quad S_{\rm QQ} = \begin{pmatrix} r'_{\rm g} & 0 & 0 \\ 0 & 0 & 0 \\ 0 & 0 & 0 \end{pmatrix}. \tag{9}$$

Equation (7) is a general combination rule for scattering matrices which appears in several scattering problems. The first term $S_{\rm PP}$ represents reflections on the terminals (only terminal 1 presents reflection for the present case). The second term comes from multiple scattering in the system. Reading from right to left, $S_{\rm QP}$ represents the transmissions to the inside region, passing through the graph and the junction $(\mathbb{1}_3 - S_{\rm QQ}S_0)^{-1}$ contains the multiple reflections between the junction and the graph, and $S_{\rm PQ}$ gives the transmissions from the internal region to the terminals.

Because it is expected that the T junction couples the terminals symmetrically, S_0 can be assumed to be symmetric. According to some measurements [29], it can be proposed as

$$S_0 = \frac{1}{3}\begin{pmatrix} -1 & 2 & 2 \\ 2 & -1 & 2 \\ 2 & 2 & -1 \end{pmatrix}. \tag{10}$$

The general structure of S is of the form

$$S = \begin{pmatrix} q_{11} & q_{12} & q_{13} \\ q_{21} & q_{22} & q_{23} \\ q_{31} & q_{32} & q_{33} \end{pmatrix}, \tag{11}$$

where $q_{ij} = S_{ij}$ for $\beta = 1$ and 2, while for $\beta = 4$

$$q_{ij} = \begin{pmatrix} S_{ij} & S_{i\bar{j}} \\ S_{\bar{i}j} & S_{\bar{i}\bar{j}} \end{pmatrix}, \tag{12}$$

where the "bar" in the subscripts denotes the corresponding terminal in the second GUE subgraph needed for the construction of the GSE graph (see Fig. 3). Therefore, the transmission coefficient from terminal j to terminal i is given by $T_{ij} = |S_{ij}|^2$ for $\beta = 1$ and 2, and $T_{ij} = \frac{1}{2}{\rm tr}(q_{ij}q_{ij}^\dagger)$ for $\beta = 4$.

Since q_{ij} is a quaternion real number, $q_{ij}q_{ij}^\dagger$ is proportional to the 2×2 unit matrix. However, in the experiment this cannot be achieved with arbitrary accuracy due to power losses. For the transmission measurements relevant to our study, they were realized within a 10% and 1% of error for q_{31} and q_{32}, respectively.

By substituting the parametrization given in Eq. (5) into Eqs. (7) to (9), and extracting the transmission coefficients T_{31} and T_{32} from Eq. (11), Eq. (3) yields

$$f = \frac{\tau - |1 + \sqrt{1-\tau}\, e^{2i\phi}|^2}{\tau + |1 + \sqrt{1-\tau}\, e^{2i\phi}|^2}, \tag{13}$$

where a and ϕ' drop out.

Using the probability density distribution of Eq. (6) the distribution of f is obtained once the integration over all parameters is done; the result is

$$p_\beta(f) = \frac{(\beta-1)!!}{\beta\,[\Gamma(\beta/2)]^2}\,\frac{(1-f)^{\beta/2}}{(1+f)^{1-\beta/2}}. \tag{14}$$

This distribution dominates for negative f values in agreement with the physical intuition since the probe at the right of the graph is closer to port 2 (see Fig. 1), making the transmission T_{32} predominantly larger than the transmission T_{31}. The width of the distribution is a signature of the nonlocal effects in the measurement of the probe port.

Equation (14) represents our main result which is valid in an ideal situation: It applies to quantum systems in the absence of any inelastic process and to classical wave systems in the absence of dissipation and imperfect coupling to the device. In Fig. 4 we show the transmissions $T_{31}(=|S_{31}|^2)$ and $T_{32}(=|S_{31}|^2)$ as a function of the frequency, obtained from the measurements of the elements of the scattering matrix S_{31} and S_{32}; for $\beta = 1$, 2, and 4. We observe that they do not reach the value of 1 due to the losses of power. Their corresponding distribution are also shown.

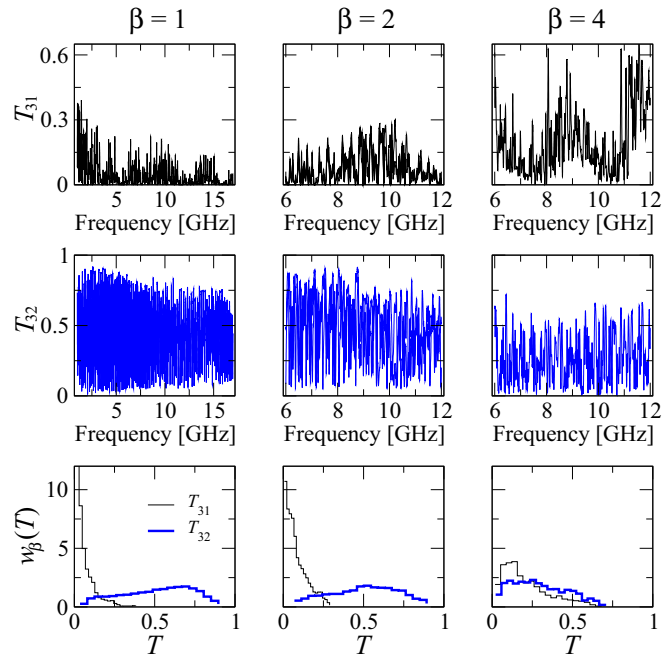

FIG. 4. Transmissions T_{31} and T_{32} as a function of frequency are shown in the upper and middle panels, and their corresponding distribution in thin black lines (thick blue lines) in the lower ones, for $\beta = 1$ (left), 2 (middle), and 4 (right), respectively.

The actual measurements for f [see Eq. (3)] are shown in Fig. 5 for experiments for the three symmetry classes: $\beta = 1$ (left panels), $\beta = 2$ (middle panels), and $\beta = 4$ (right panels). In the upper panels we show the fluctuations of f as a function of the frequency for the three-terminal microwave setup of Fig. 1. For $\beta = 1$, the spectrum was measured in the frequency range from 1 to 17 GHz, while for $\beta = 2$ and 4 the interval from 6 to 12 GHz was considered due to the range of operation of the circulators. In the lower panels the experimental distribution of f is shown as histograms. The solid lines correspond to the theoretical expectation, see Eq. (14).

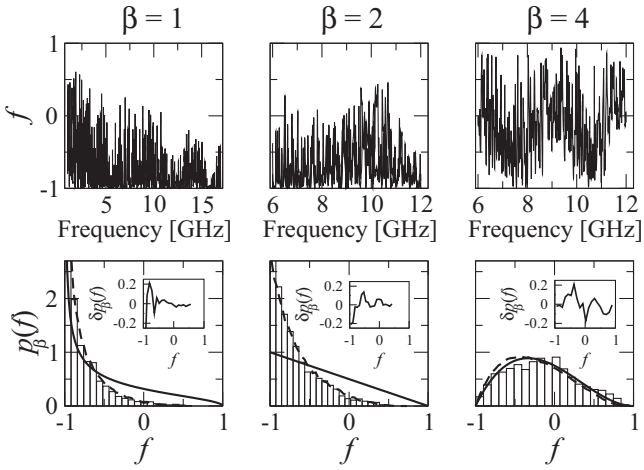

FIG. 5. f as a function of the frequency is shown in the upper panels, and its corresponding distribution in the lower ones, for $\beta = 1$ (left), 2 (middle), and 4 (right). In the lower panels the continuous lines represent the analytical result for the ideal case, Eq. (14), while the dashed lines correspond to RMT simulations with power losses and imperfect coupling of the T junctions to the graph, where all parameters were fixed before hand using the autocorrelation functions (see Fig. 6). In the insets the difference between the numerical and the experimental distribution $\delta p_\beta(f) = p_\beta(f)_{\rm num} - p_\beta(f)_{\rm expt}$ are presented for comparison purposes. For the statistical analysis we used an ensemble of 5×10^4 realizations.

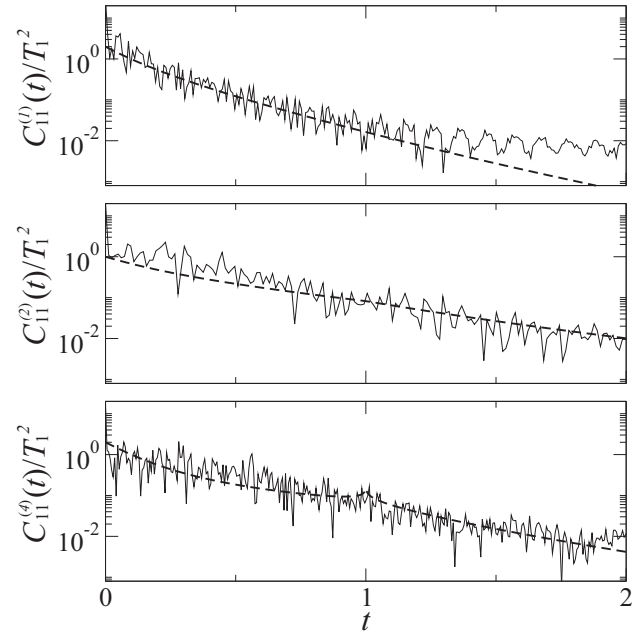

FIG. 6. Fitting of the autocorrelation function Eq. (16) to the experimental data. The parameters are $T_1 = 0.98$ and $\gamma = 1.9$ for $\beta = 1$, $T_1 = 0.96$ and $\gamma = 0.5$ for $\beta = 2$, and $T_1 = 0.97$ and $\gamma = 0.2$ for $\beta = 4$.

The deviations between experiment and theory observed for the cases $\beta = 1$ and 2 can be explained by the power losses and the imperfect coupling between the graph and the ports. The effect of the absorption can be quantified by assuming that the scattering matrix of the graph does not conserve flux; while imperfect coupling can be modeled by adding identical barriers, with transmission intensity T_a, between the graph and port 1, between the graph and the T junction, and between the T junction and port 2, respectively. Following Ref. [6], such scattering matrix, which we denote by $\widetilde{S}_{\rm g}$, can be written as

$$\widetilde{S}_{\rm g}(E) = 1 - 2\pi {\rm i}\widetilde{W}^\dagger \frac{1}{E - \widetilde{\mathcal{H}} + {\rm i}\pi \widetilde{W}\widetilde{W}^\dagger}\widetilde{W}, \qquad (15)$$

where E is the energy and $\widetilde{W}$ accounts for the coupling between the resonant modes of the graph and the scattering channels. Here $\widetilde{\mathcal{H}}_{mn} = H_{mn} + {\rm i}(\gamma\Delta/4\pi)\delta_{mn}$, with H being the Hamiltonian that describes the closed microwave graph with mean level spacing Δ and it is taken from the Gaussian ensembles corresponding to the symmetry present in the graph. The imaginary part of $\widetilde{\mathcal{H}}$ mimics the absorption quantified by the parameter γ. It can be extracted from the experimental data through the autocorrelation function $C_{\rm ab}^{(\beta)}(t)$ between the elements of the scattering matrix $S_{\rm ab}$. The corresponding expression for the GOE is given in Ref. [30], while for all β in Ref. [31]. After some mathematics, they can be written for the element S_{11} as

$$\frac{C_{11}^{(\beta)}(t)}{T_1^2} = \begin{cases} \left[\frac{3}{(1+2T_1 t)^3} - \frac{b_{1,2}(t)}{(1+T_1 t)^4}\right]e^{-\gamma t} & \text{for } \beta = 1, \\ \left[\frac{2}{(1+T_1 t)^4} - \frac{2^6\, b_{2,2}(t)}{(2+T_1 t)^6}\right]e^{-\gamma t} & \text{for } \beta = 2, \\ \left[\frac{6}{(1+T_1 t)^6} - \frac{2^{12}\, b_{4,2}(t)}{(2+T_1 t)^{10}}\right]e^{-2\gamma t} & \text{for } \beta = 4, \end{cases} \qquad (16)$$

where $b_{\beta,2}(t)$ is the two-level form factor [32] and T_1 is the coupling strength, which is also extracted from the experiment via $T_1 = 1 - |\langle S_{11}\rangle|^2$ with the average $\langle S_{11}\rangle$ taken over the frequency.

In Fig. 6 we show the autocorrelation function $C_{11}^{(\beta)}(t)$ of the experimental data. The best fit yields $T_1 = 0.98$ and $\gamma = 1.9$ for $\beta = 1$, $T_1 = 0.96$ and $\gamma = 0.5$ for $\beta = 2$, and $T_1 = 0.97$ and $\gamma = 0.2$ for $\beta = 4$, and they are plotted as dashed lines. As expected the coupling parameters are almost the same for the three symmetries but the absorption parameter is significantly different from one symmetry to another. In particular, we notice that the value of γ for $\beta = 2$ is almost twice the value for $\beta = 4$. This may be due to the interplay between reflection and absorption [33], i.e., the higher the reflection the smaller the absorption, and also due to the fact that γ is given in units of Δ which is not the same for all graphs. This is the situation of the $\beta = 4$ case which presents twice the reflection than that of the $\beta = 2$ case (two subgraphs). Also, the circulators introduce more reflections for $\beta = 2$ and 4 in comparison with the $\beta = 1$ case with no circulators. The parameters T_1 and γ are used in Eq. (15), from which we obtain T_{31} and T_{32}, and finally compute f. The results are shown in Fig. 5 (lower panels) as dashed lines. A good agreement with the experimental distribution is observed. For the symplectic case the agreement between experiment and theory is good even without the correction due to absorption and imperfect coupling; since γ is relatively small, $p_4(f)$ depends only weakly on the port couplings which are almost perfect.

To conclude, we used three-terminal chaotic microwave graphs to measure the different transmissions to extract the quantity f that accounts for the voltage drop in an equivalent quantum device and exhibits its nonlocal effects. We success-

fully described the experimentally obtained distribution $p(f)$ providing analytical expressions for the ideal case, for the three symmetry classes. Deviations from the ideal case for the orthogonal and unitary symmetries are due to the presence of dissipation and imperfect coupling between the graph and the junctions. Surprisingly, the dissipation and the coupling strength do not erase the fingerprints of the symplectic symmetry. We expect that our results motivate further studies for a successful explanation of robustness of symplectic symmetry for imperfect couplings and higher dissipation.

A.M.M.-A. acknowledges financial support from PRODEP under the project DSA/103.5/16/11850. This work was partially supported by Fondo Institucional PIFCA (Grant No. BUAP-CA-169), and CONACyT (Grants No. CB-2013/220624 and No. CB-2016/285776). The experiments were funded by the Deutsche Forschungsgemeinschaft via the individual grants STO 157/17-1 and KU 1525/3-1 including a short-term visit of A.M.M.-A. in Marburg.

[1] J. Phys. A: Math. Gen. **38** (2005), edited by Y. V. Fyodorov, T. Kottos, and H.-J. Stöckmann, Special issue on Trends in Quantum Chaotic Scattering.
[2] P. A. Mello and N. Kumar, *Quantum Transport in Mesoscopic Systems: Complexity and Statistical Fluctuations* (Oxford University Press, Oxford, 2004).
[3] M. Büttiker, Phys. Rev. Lett. **57**, 1761 (1986).
[4] M. Büttiker, IBM, J. Res. Dev. **32**, 317 (1988).
[5] R. Landauer, J. Phys.: Condens. Matter **1**, 8099 (1989).
[6] P. W. Brouwer and C. W. J. Beenakker, Phys Rev. B **55**, 4695 (1997).
[7] H. Schanze, E. R. P. Alves, C. H. Lewenkopf, and H. J. Stöckmann, Phys. Rev. E **64**, 065201(R) (2001).
[8] H. Schanze, H.-J. Stöckmann, M. Martínez-Mares, and C. H. Lewenkopf, Phys. Rev. E **71**, 016223 (2005).
[9] M. Martínez-Mares, Phys. Rev. E **72**, 036202 (2005).
[10] E. Flores-Olmedo, A. M. Martínez-Argüello, M. Martínez-Mares, G. Báez, J. A. Franco-Villafañe, and R. A. Méndez-Sánchez, Sci. Rep. **6**, 25157 (2016).
[11] E. Doron, U. Smilansky, and A. Frenkel, Phys. Rev. Lett. **65**, 3072 (1990).
[12] R. A. Méndez-Sánchez, U. Kuhl, M. Barth, C. H. Lewenkopf, and H.-J. Stöckmann, Phys. Rev. Lett. **91**, 174102 (2003).
[13] U. Kuhl, M. Martínez-Mares, R. A. Méndez-Sánchez, and H.-J. Stöckmann, Phys. Rev. Lett. **94**, 144101 (2005).
[14] J. Barthélemy, O. Legrand, and F. Mortessagne, Phys. Rev. E **71**, 016205 (2005).
[15] S. Hemmady, X. Zheng, E. Ott, T. M. Antonsen, and S. M. Anlage, Phys. Rev. Lett. **94**, 014102 (2005).
[16] O. Hul, O. Tymoshchuk, S. Bauch, P. M. Koch, and L. Sirko, J. Phys. A: Math. Gen. **38**, 10489 (2005).
[17] P. So, S. M. Anlage, E. Ott, and R. N. Oerter, Phys. Rev. Lett. **74**, 2662 (1995).
[18] U. Stoffregen, J. Stein, H.-J. Stöckmann, M. Kuś, and F. Haake, Phys. Rev. Lett. **74**, 2666 (1995).
[19] F. Kuemmeth, K. I. Bolotin, S.-F. Shi, and D. C. Ralph, Nano Lett. **8**, 4506 (2008).
[20] A. Rehemanjiang, M. Allgaier, C. H. Joyner, S. Müller, M. Sieber, U. Kuhl, and H.-J. Stöckmann, Phys. Rev. Lett. **117**, 064101 (2016).
[21] A. Rehemanjiang, M. Richter, U. Kuhl, and H.-J. Stöckmann, Phys. Rev. E **97**, 022204 (2018).
[22] S. Datta, *Electronic Transport in Mesoscopic Systems* (Cambridge University Press, Cambridge, 1995).
[23] S. Godoy and P. A. Mello, Europhys. Lett. **17**, 243 (1992).
[24] S. Godoy and P. A. Mello, Phys. Rev. B **46**, 2346 (1992).
[25] F. J. Dyson, J. Math. Phys. **3**, 140 (1962).
[26] F. Haake, *Quantum Signatures of Chaos. 2nd edition* (Springer, Berlin, 2001).
[27] P. W. Brouwer and C. W. J. Beenakker, Phys. Rev. B **50**, 11263 (1994).
[28] A. M. Martínez-Argüello, E. Castaño, and M. Martínez-Mares, AIP Conf. Proc. **46**, 1579 (2014).
[29] M. Allgaier, S. Gehler, S. Barkhofen, H.-J. Stöckmann, and U. Kuhl, Phys. Rev. E **89**, 022925 (2014).
[30] R. Schäfer, T. Gorin, T. H. Seligman, and H.-J. Stöckmann, J. Phys. A: Math. Gen. **36**, 3289 (2003).
[31] Y. V. Fyodorov, D. V. Savin, and H.-J. Sommers, J. Phys. A: Math. Gen. **38**, 10731 (2005).
[32] T. Guhr, A. Müller-Groeling, and H. A. Weidenmüller, Phys. Rep. **229**, 189 (1998).
[33] G. Báez, M. Martínez-Mares, and R. A. Méndez-Sánchez, Phys. Rev. E **78**, 036208 (2008).